



Supplement of

Ice-nucleating particle concentration measurements from Ny-Ålesund during the Arctic spring–summer in 2018

Matteo Rinaldi et al.

Correspondence to: Matteo Rinaldi (m.rinaldi@isac.cnr.it)

The copyright of individual parts of the supplement might differ from the article licence.

Contents of this file

Table S1

Figures S1 to S16.

Sect S1. Considerations on the robustness of the *n*INP-CHL correlation maps.

Table S1. Summary of sampling conditions for filters collected for WT-CRAFT.

Sample ID	Filter Sampling Ref Start Time	Filter Sampling Ref End Time	Flow Rate	Air Volume	Suspension water volume	nINP corresponding to the first frozen droplet
	DAT.UTC	DAT.UTC	LPM	L	mL	m ³
NYA_GVB_01	4/16/2018 17:00	4/20/2018 10:00	5.100	13617.000	2.84	1.00
NYA_GVB_02	4/20/2018 14:40	4/24/2018 14:40	5.070	14601.600	3.08	1.01
NYA_GVB_03	4/24/2018 18:20	4/28/2018 16:00	5.450	15314.500	3.10	0.97
NYA_GVB_04	4/29/2018 13:30	5/2/2018 16:15	5.550	12445.875	2.42	0.93
NYA_GVB_05	5/2/2018 16:20	5/6/2018 14:37	5.470	15471.895	3.26	1.01
NYA_GVB_06	5/6/2018 14:45	5/10/2018 13:00	5.420	15325.050	3.26	1.02
NYA_GVB_07	5/10/2018 13:10	5/14/2018 11:05	5.640	15890.700	3.29	0.99
NYA_GVB_08	5/14/2018 11:15	5/18/2018 7:50	5.465	15179.037	3.10	0.98
NYA_GVB_09	5/18/2018 8:00	5/22/2018 8:28	5.500	15917.000	3.32	1.00
NYA_GVB_10	5/22/2018 8:30	5/26/2018 11:33	4.800	14263.200	2.98	1.00
NYA_GVB_21	5/26/2018 11:45	6/3/2018 18:30	5.515	32883.188	6.86	1.00
NYA_GVB_22	6/3/2018 18:35	6/7/2018 17:20	5.480	15576.900	3.25	1.00
NYA_GVB_23	6/7/2018 17:24	6/11/2018 17:35	5.430	15668.265	3.27	1.00
NYA_GVB_24	6/11/2018 17:40	6/15/2018 16:24	5.355	15218.910	3.18	1.00
NYA_GVB_25	6/15/2018 16:28	6/19/2018 19:05	5.370	15887.145	3.32	1.00
NYA_GVB_26	6/19/2018 19:09	6/23/2018 19:16	5.255	15152.792	3.16	1.00
NYA_GVB_27	6/23/2018 19:20	6/27/2018 13:55	5.345	14525.037	3.03	1.00
NYA_GVB_28	6/27/2018 14:00	7/1/2018 16:40	5.410	16013.600	3.34	1.00
NYA_GVB_16	7/1/2018 16:50	7/5/2018 17:20	5.455	15792.225	3.30	1.00
NYA_GVB_17	7/5/2018 17:25	7/9/2018 17:22	5.415	15587.078	3.25	1.00
NYA_GVB_18	7/9/2018 17:27	7/13/2018 18:24	5.385	15662.273	3.27	1.00
NYA_GVB_19	7/13/2018 18:33	7/17/2018 16:43	5.335	15071.375	3.15	1.00
NYA_GVB_20	7/17/2018 16:52	7/21/2018 15:55	5.345	15241.268	3.18	1.00
NYA_GVB_11	7/21/2018 16:02	7/25/2018 16:31	5.395	15602.340	3.26	1.00
NYA_GVB_12	7/25/2018 16:38	7/29/2018 15:07	5.430	15391.334	3.21	1.00
NYA_GVB_13	7/29/2018 15:14	8/2/2018 18:39	5.450	16254.626	3.39	1.00
NYA_GVB_14	8/7/2018 15:55	8/11/2018 14:05	5.445	15382.126	3.21	1.00
NYA_GVB_15	8/11/2018 14:12	8/15/2018 17:36	5.425	16177.350	3.38	1.00

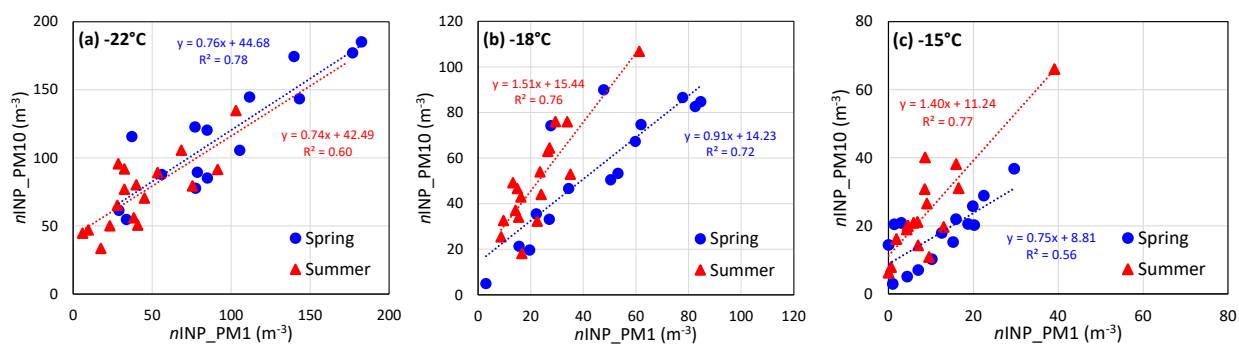


Figure S1. Scatter plot between PM_1 and PM_{10} $nINP$ (measured by DFPC) at T of -22°C (a), -18°C (b) and -15°C (c).

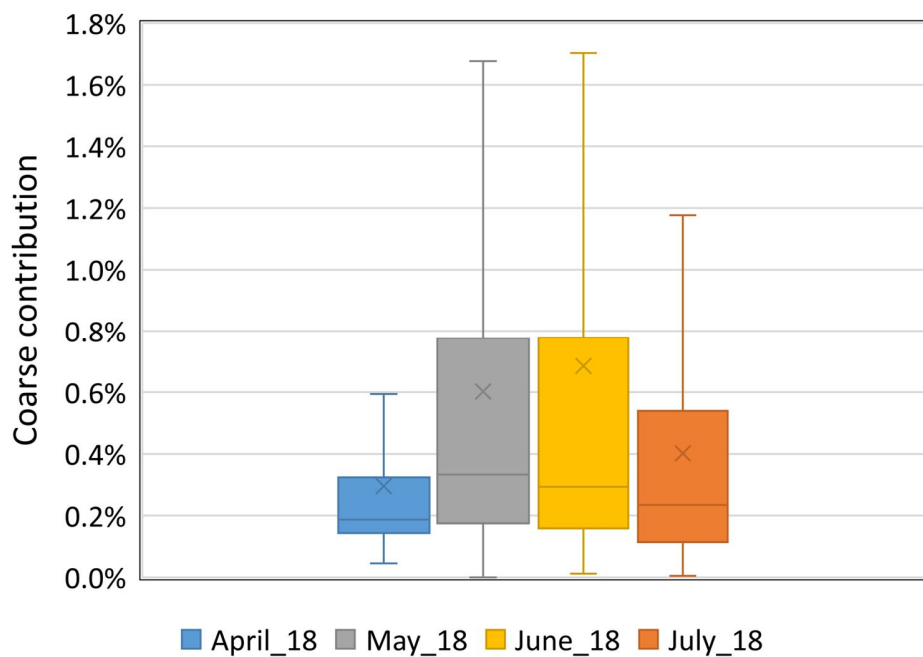


Figure S2: Contribution of super-micrometer aerosol particles (coarse fraction) to the 0.1-10 μm size range in April, May, June and July 2018. The cross symbols indicate the average, the mid lines indicate the median, the boxes enclose the 25th and 75th percentiles while the whiskers indicates the 5th and 95th percentiles.

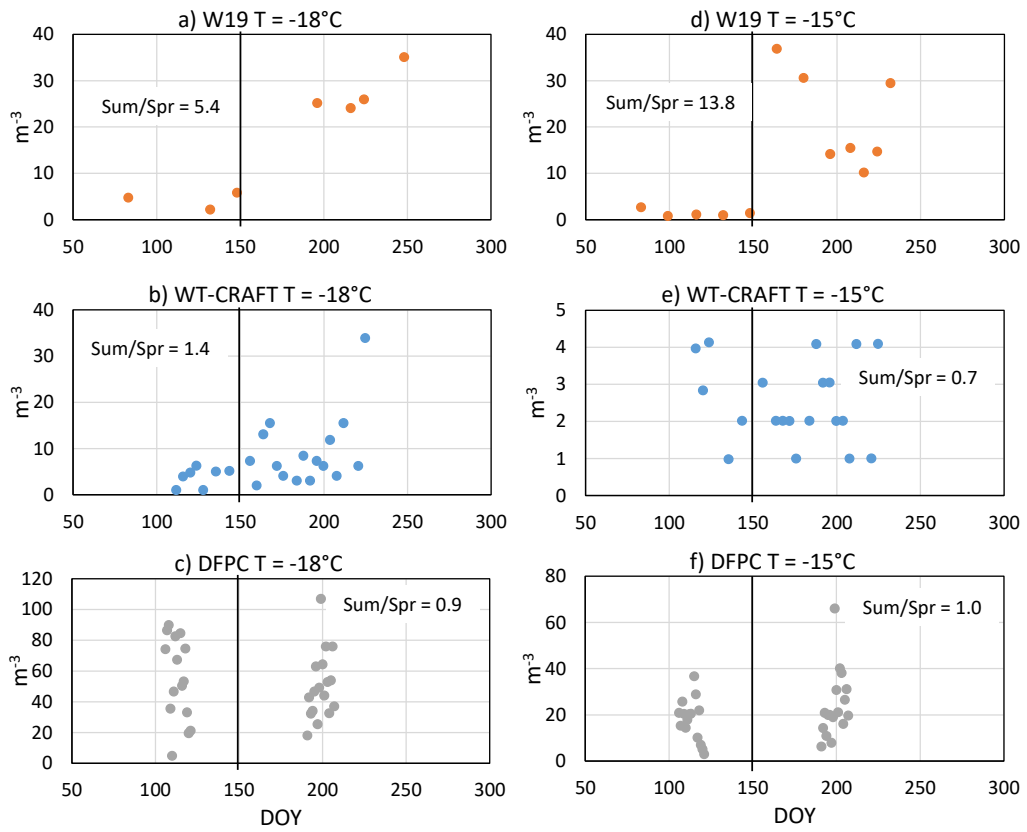


Figure S3. Seasonal evolution of $nINP$ in this study (GVB, 2018) compared to the results by Wex et al. (2019), here indicated as W19, obtained at GVB in spring-summer 2012.

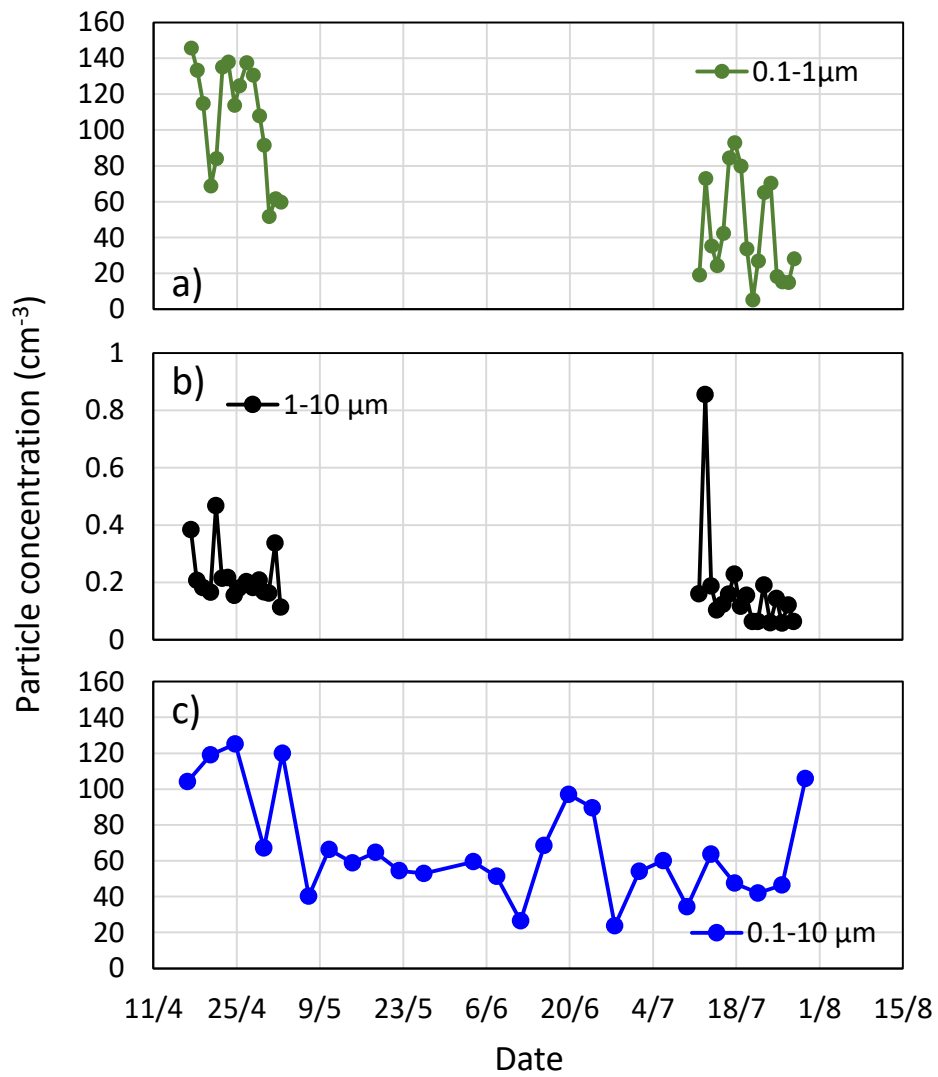


Figure S4. Particle number concentration data averaged over the INP sampling times. (a) size range between 0.1 and 1 μm averaged over the DFPC sampling times; (b) size range between 1 and 10 μm averaged over the DFPC sampling times; (c) size range between 0.1 and 10 μm averaged over the WT-CRAT sampling times.

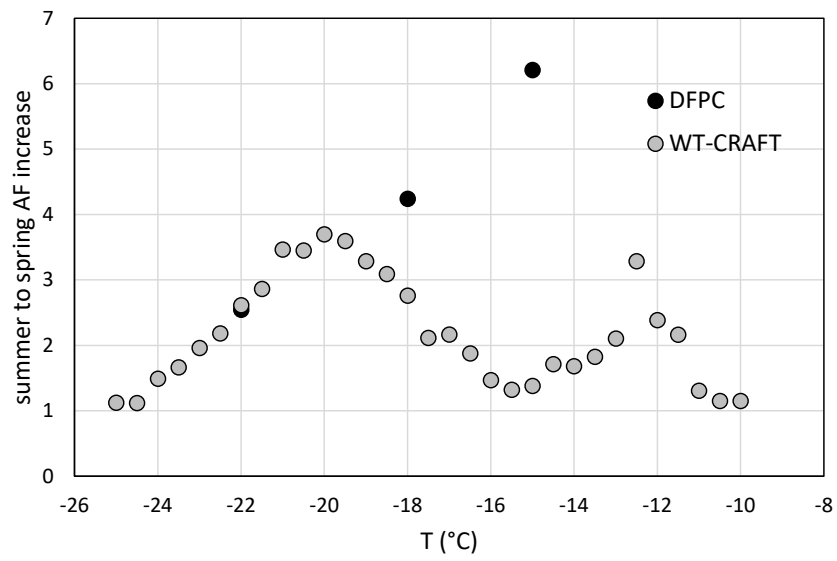


Figure S5. Spring to summer AF increase for DFPC and WT-CRAFT data. AF data for DFPC are derived from PM₁₀ data.

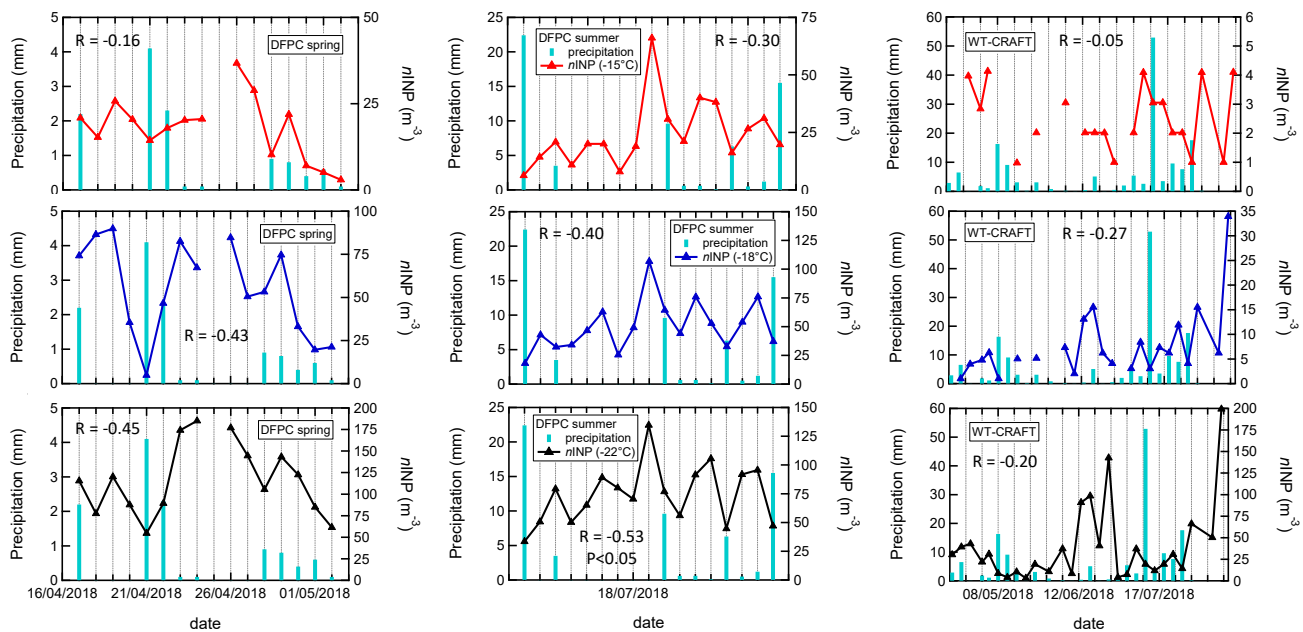


Figure S6: Impact of precipitation events on nINP at GVB during 2018. Each plot represents the nINP (PM₁₀) time series together with the average precipitations occurred during the sampling; the Pearson correlation coefficient between nINP and precipitation is also reported (when the correlation is statistically significant, the significance level, p, is also reported).

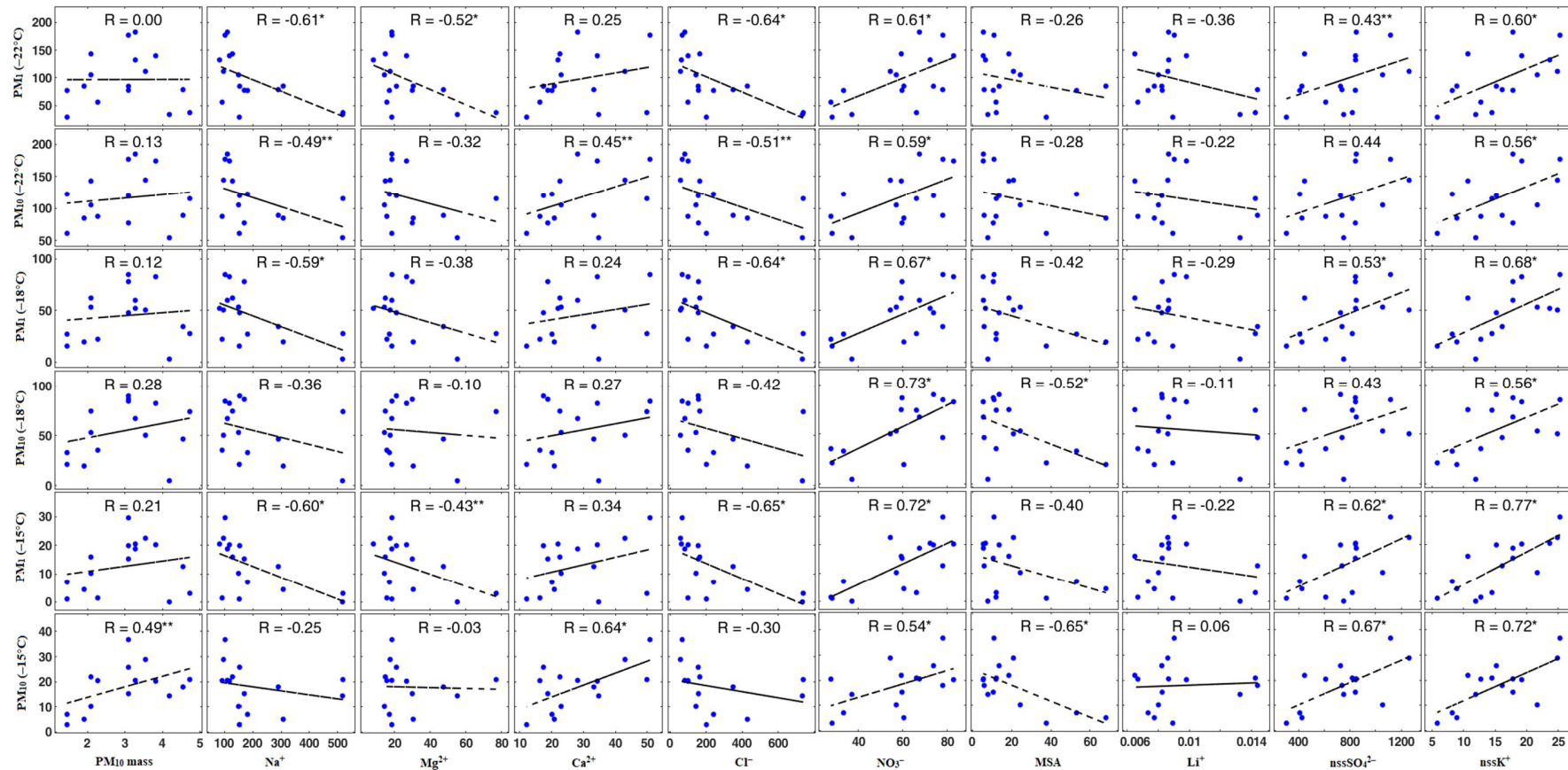


Figure S7. Scatter plots between $n\text{INP}_{\text{DFFC}}$ (y axis) and chemical tracers (x axis), during the spring campaign. $n\text{INP}$ is expressed in units of m^{-3} , chemical tracers are expressed as ng m^{-3} , while PM_{10} mass is in $\mu\text{g m}^{-3}$.

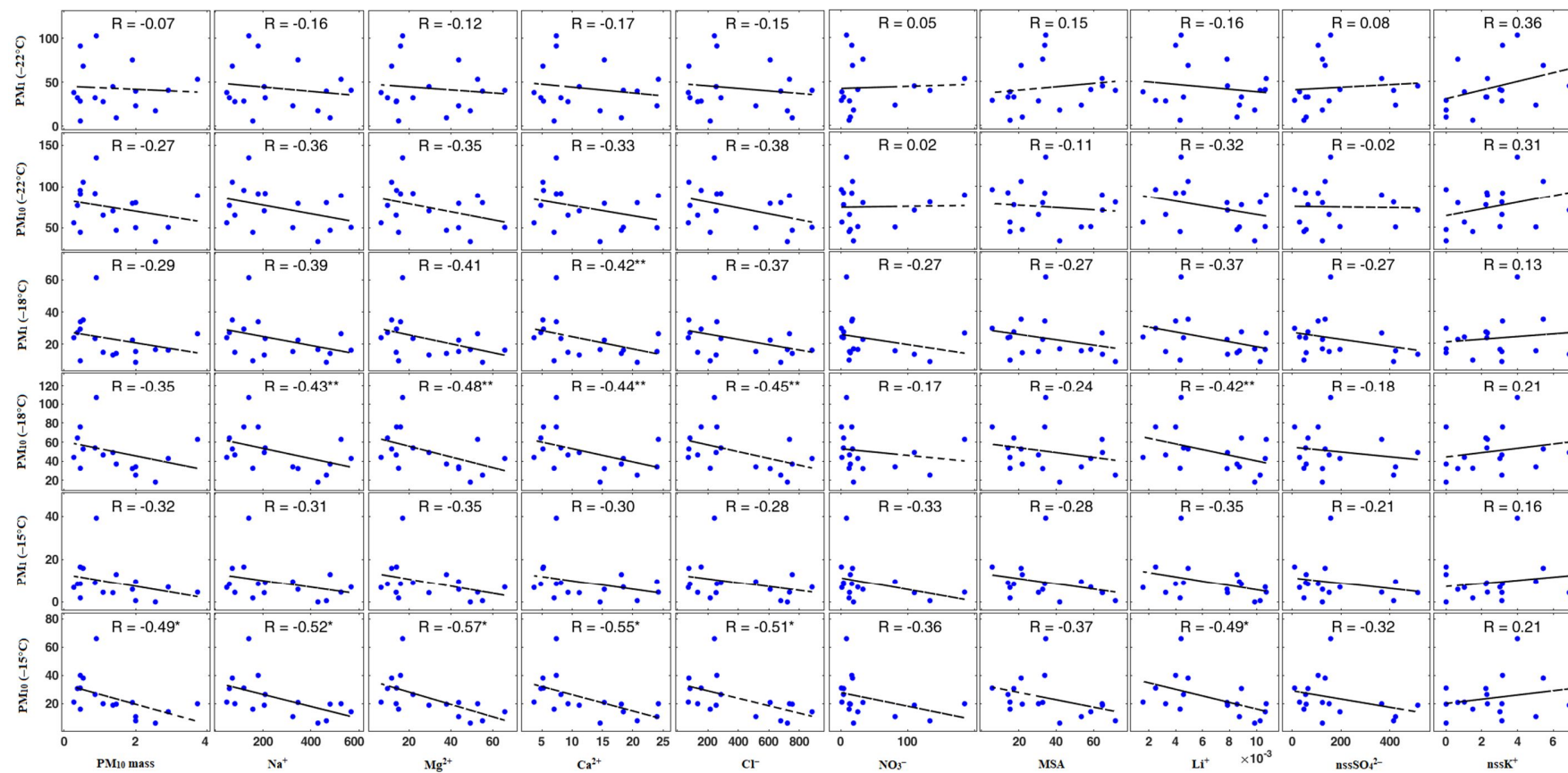


Figure S8. Scatter plots between $nINP_{DFFC}$ (y axis) and chemical tracers (x axis) during the summer campaign. $nINP$ is expressed in units of m^{-3} , chemical tracers are expressed as $ng\ m^{-3}$, while PM_{10} mass is in $\mu g\ m^{-3}$.

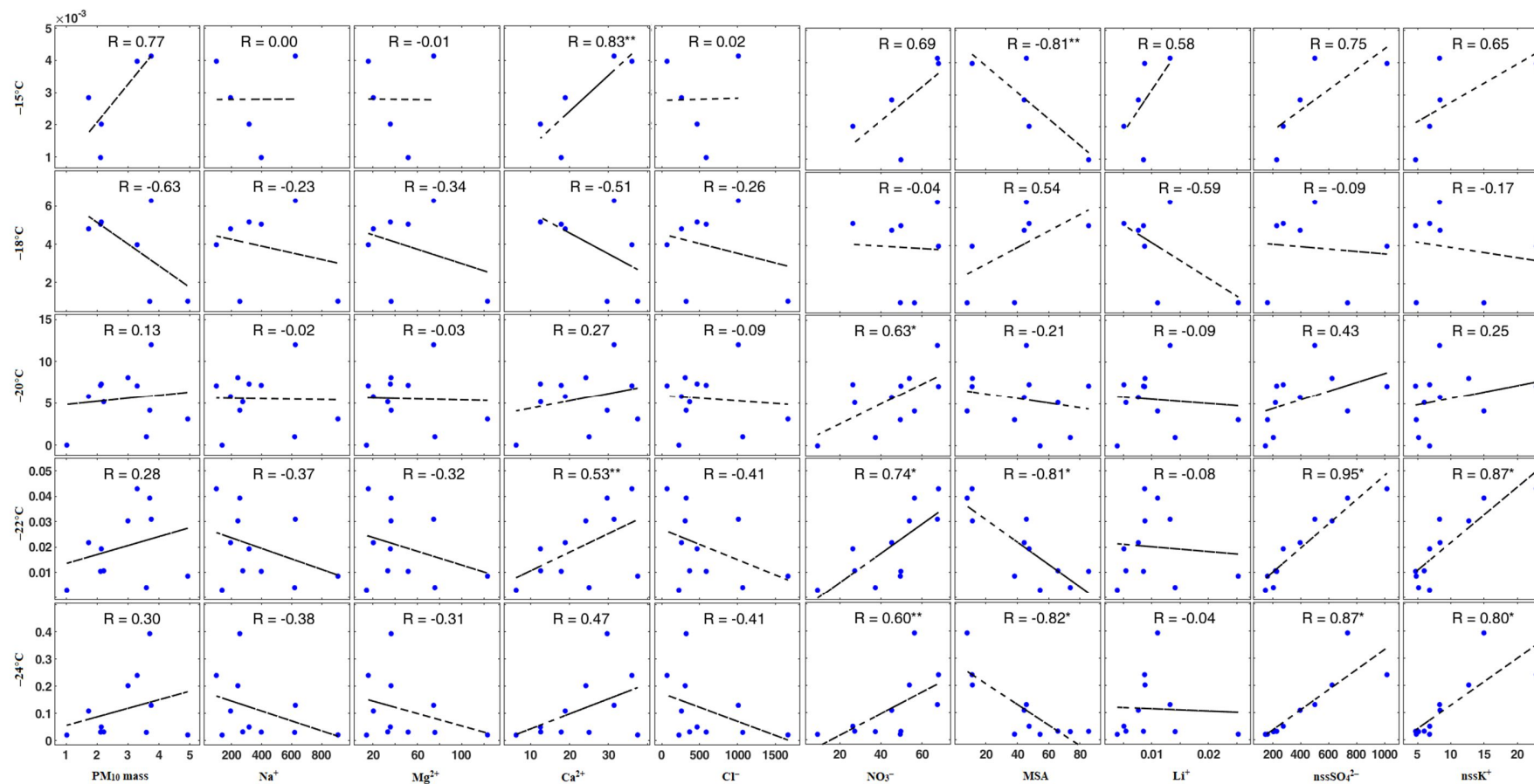


Figure S9. Scatter plots between $nINP_{WT-CRAFT}$ (y axis) and chemical tracers (x axis) during the spring campaign. $nINP$ is expressed in units of m^{-3} , chemical tracers are expressed as $ng\ m^{-3}$, while PM_{10} mass is in $\mu g\ m^{-3}$.

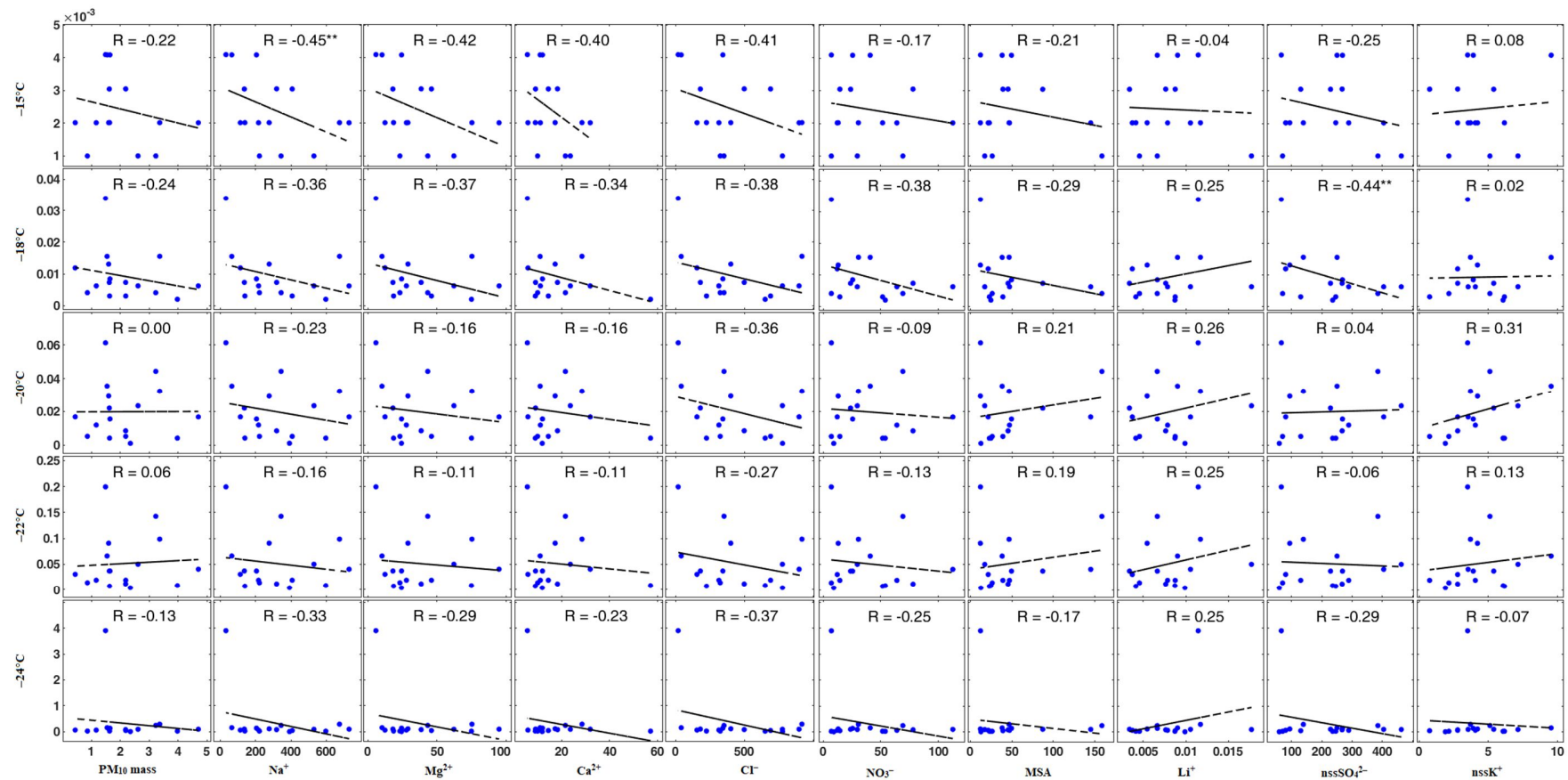


Figure S10. Scatter plots between $nINP_{WT-CRAFT}$ (y axis) and chemical tracers (x axis) during the summer campaign. $nINP$ is expressed in units of m^{-3} , chemical tracers are expressed as $ng\ m^{-3}$, while PM_{10} mass is in $\mu g\ m^{-3}$.

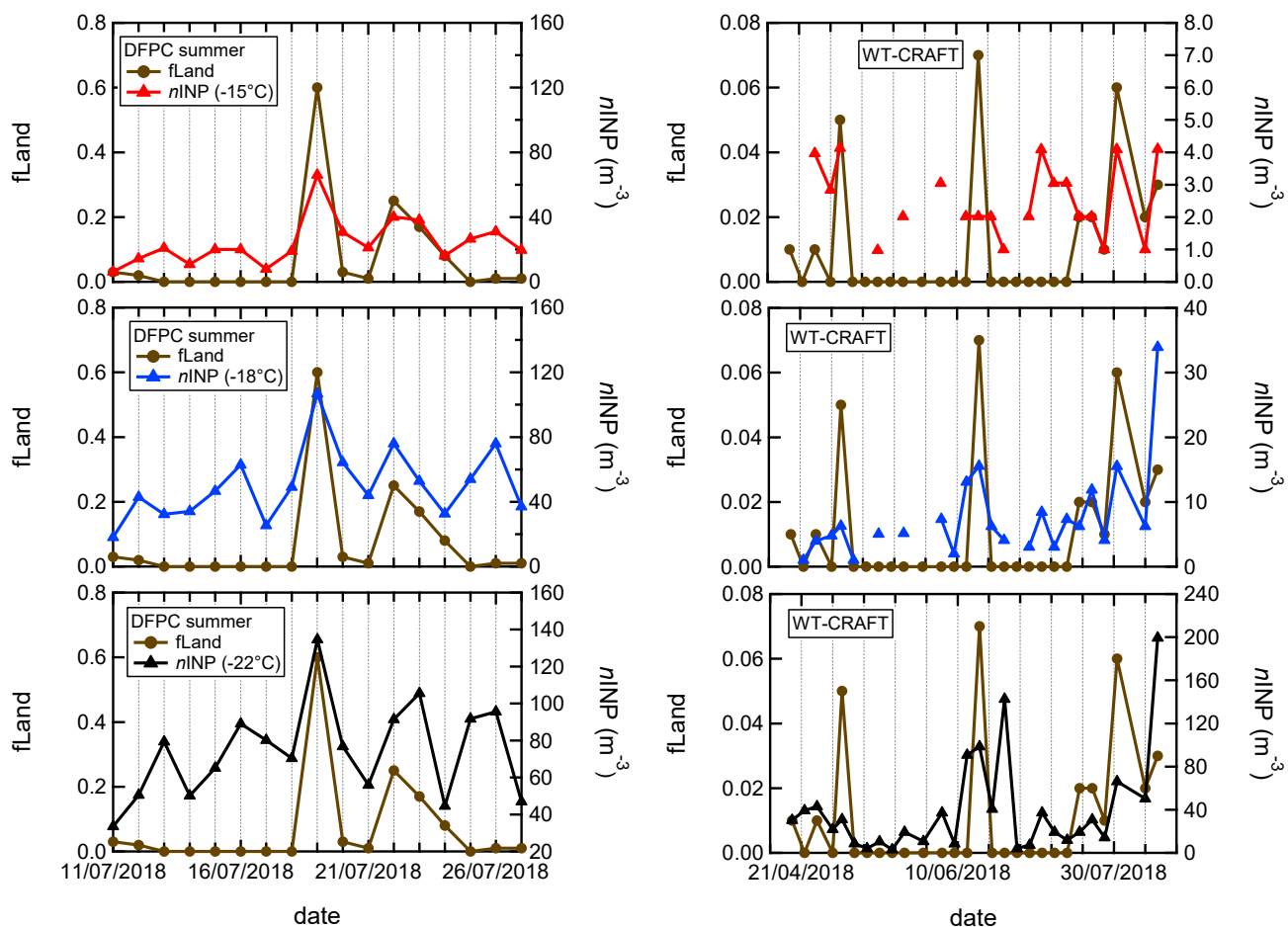


Figure S11: Influence of the “Land” ground type (fLand) during the DFPC summer (left) and WT-CRAFT (right) campaigns overlapped with the INP atmospheric concentrations at T of -15, -18 and -22°C.

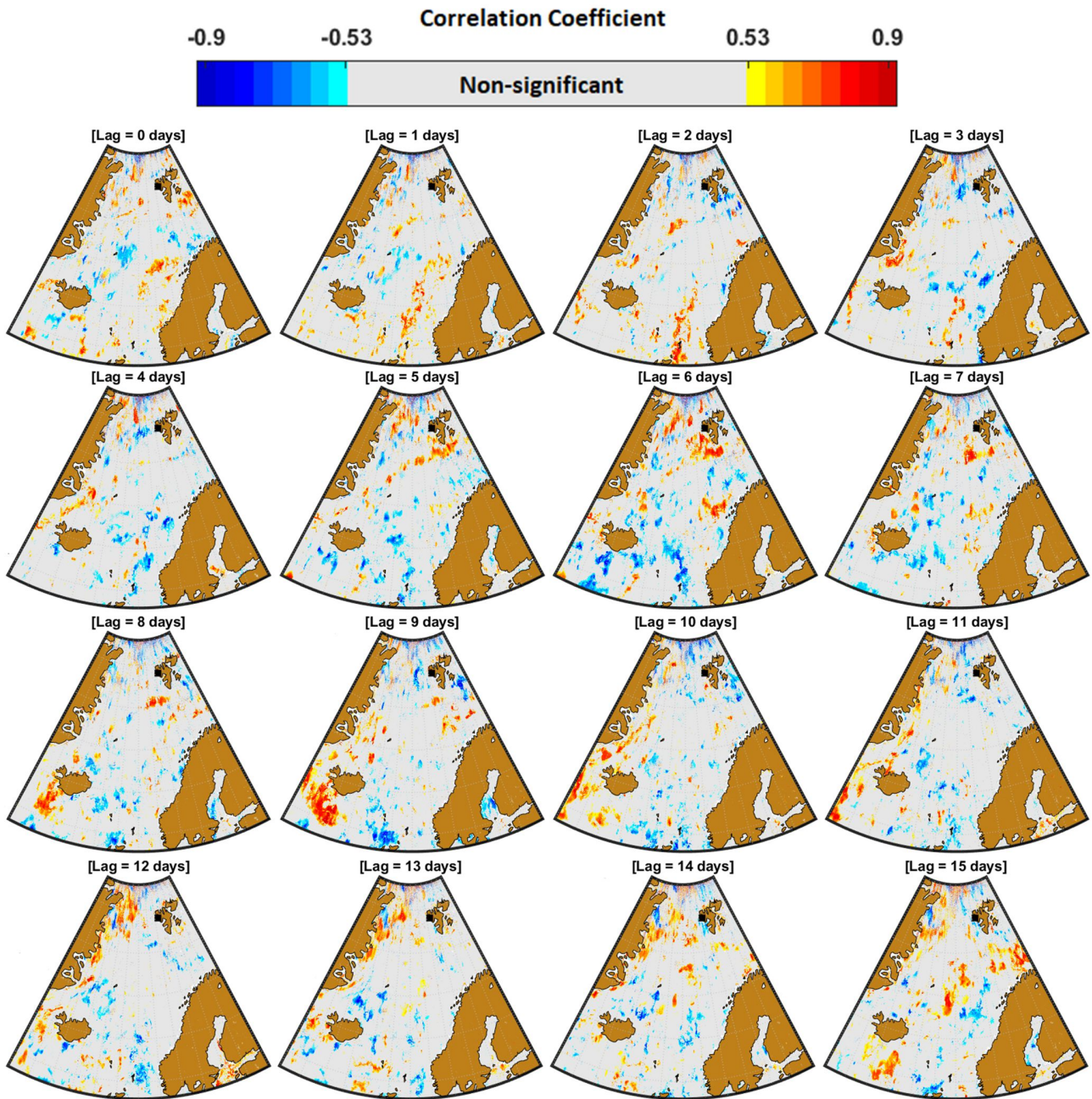


Figure S12: Spatial distribution of the correlation coefficient between DFPC $nINP_{PM1}$ [$T = -15\text{ }^{\circ}\text{C}$] sampled at GVB in Summer 2018 and CHL over the Arctic Ocean at different time-lags from 0 to 27 days. The grey color represents non-significant correlation coefficients ($p < 0.05$). The 3 samples with land influences were excluded from the analysis.

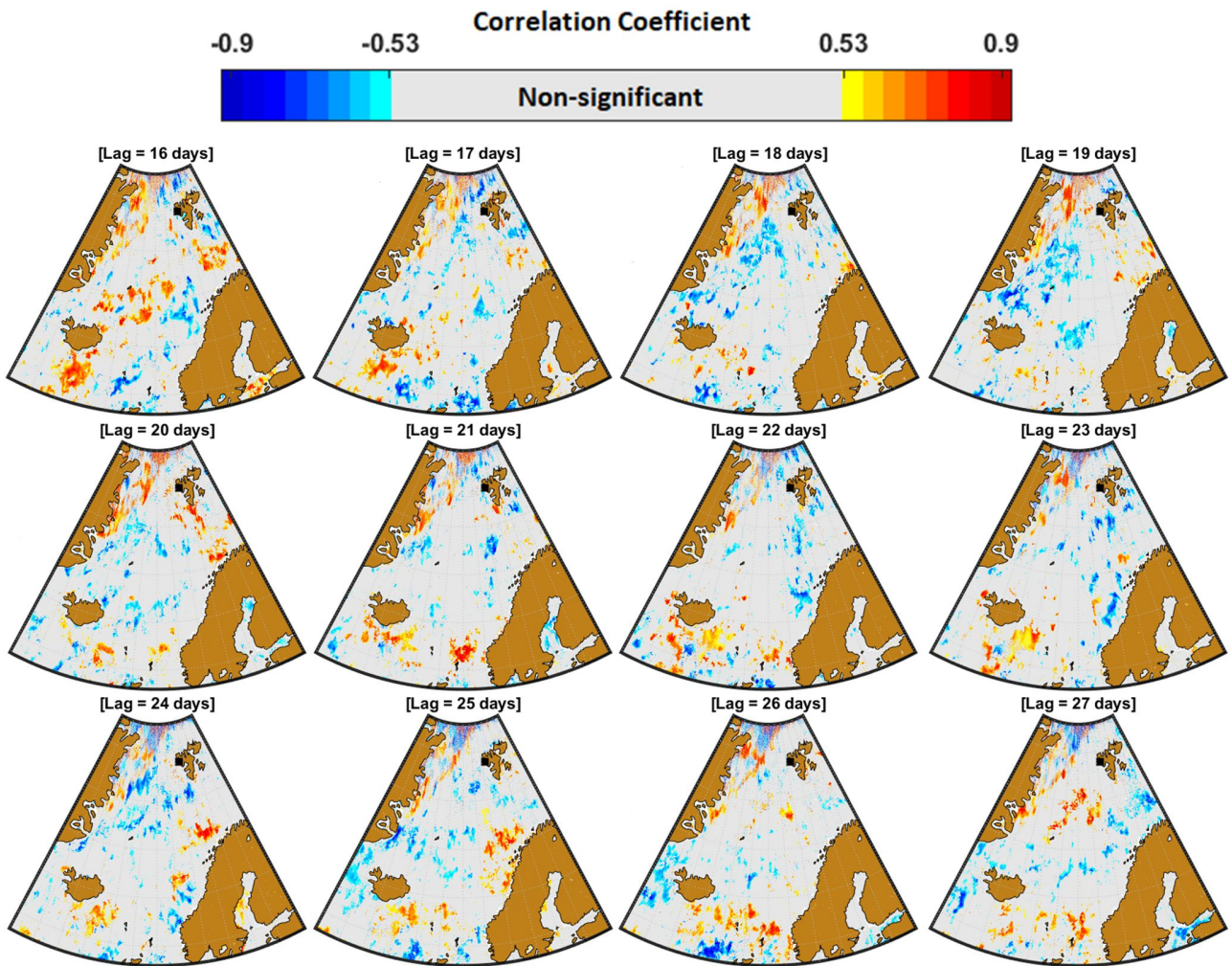


Figure S12: Continued.

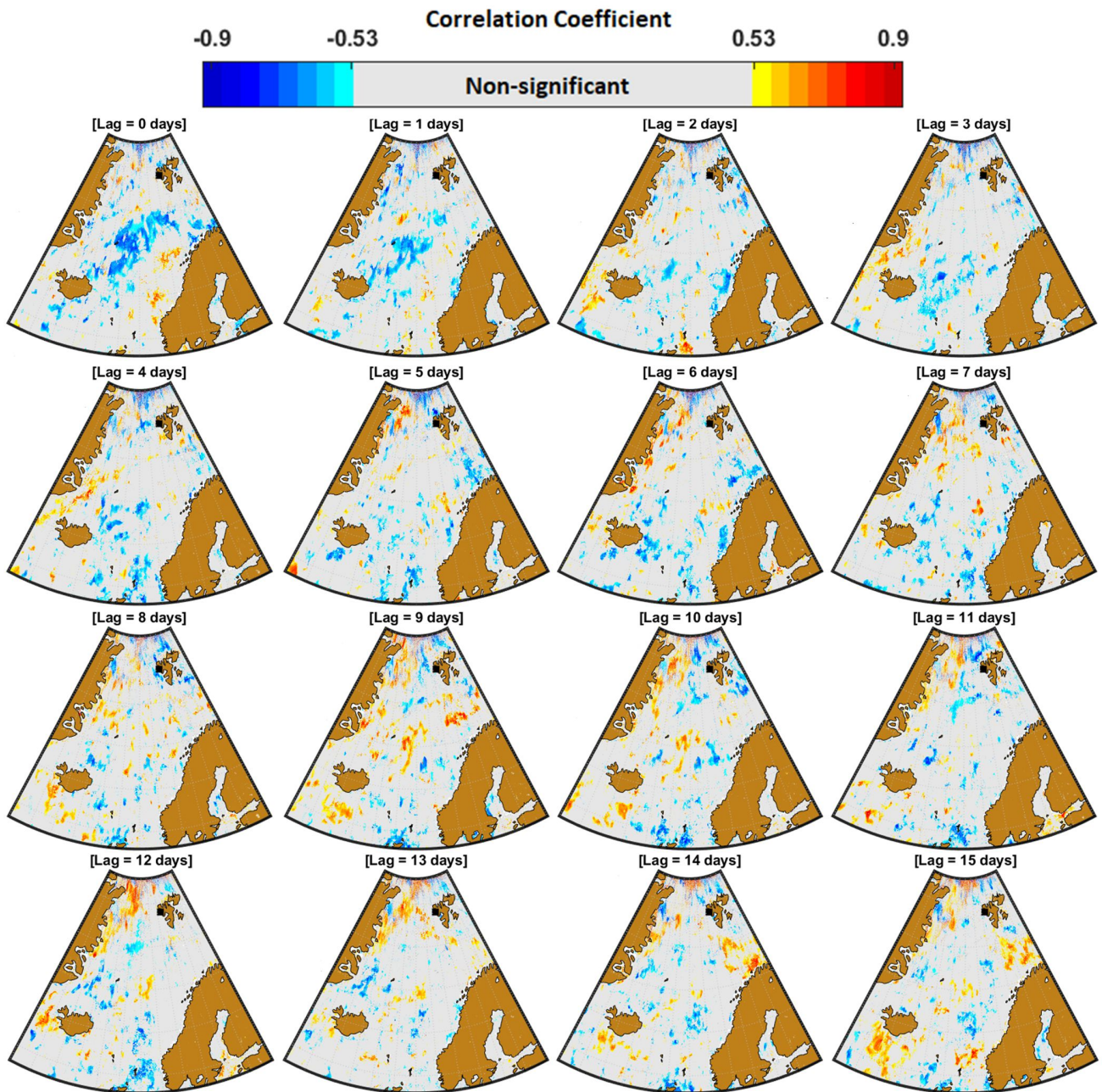


Figure S13: Spatial distribution of the correlation coefficient between DFPC $nINPM_{10}$ [$T = -15\text{ }^{\circ}\text{C}$] sampled at GVB in Summer 2018 and CHL over the Arctic Ocean at different time-lags from 0 to 27 days. The grey color represents non-significant correlation coefficients ($p < 0.05$). The 3 samples with land influences were excluded from the analysis.

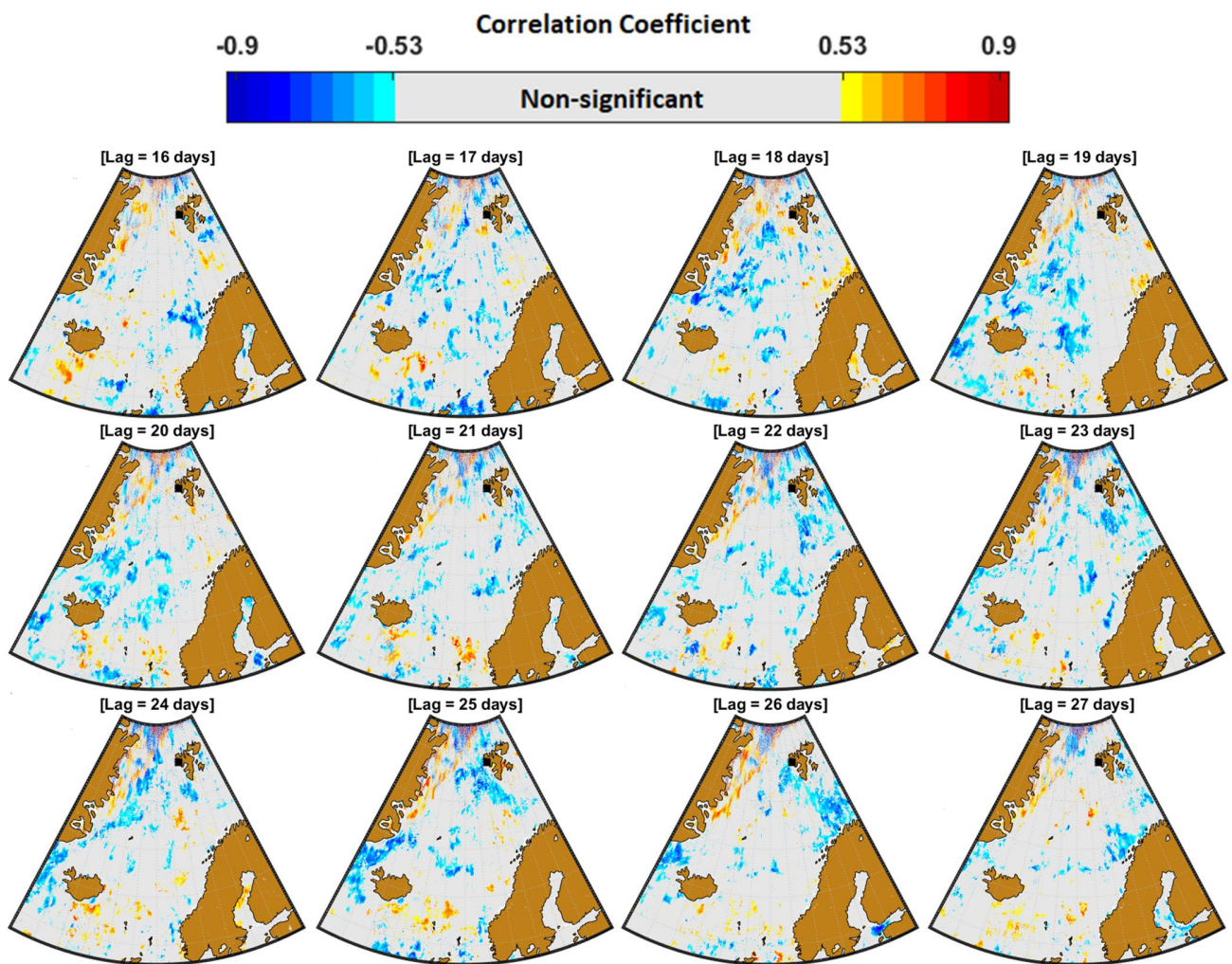


Figure S13: Continued.

S1. Considerations on the robustness of the *n*INP-CHL correlation maps

Considering the limited number of data points (14 samples) used in the spatio-temporal correlation analysis, we carefully evaluated the robustness of the correlations that originate the obtained correlation maps (Figure 7 in the manuscript). It is impossible to check visually all the regressions that form the correlation maps discussed here as each map is composed of 651,508 pixels, of which between 30,724 (~ 5%) and 85,829 (~ 13%) present a positive and significant correlation, according to the considered delay time from 0 to 27 day. Therefore, we focused on the three evidenced sea regions characterized by systematic high correlation between INP and CHL (evidenced in Figure 7) and we divided, within each region, the significant and positively correlating pixels into three categories: High, Medium, and Low correlating, according to the distribution of the correlation coefficient. Then we selected randomly 6 pixels within each category, per each region, of which we plotted the results of the INP vs. CHL regression analysis, for a total of 54 scatter plots (Figure S7, Figure S8 and Figure S9). Careful investigation of the randomly selected scatter plots shows a variety of conditions regarding the robustness of the investigated correlation, with generally robust correlations, in the majority of the cases not distorted (or influenced) by one single (or a few) points, which we consider a prove of the robustness of the obtained correlation maps.

Category

Region 1 [75° – 78° N and 0° – 18° E]

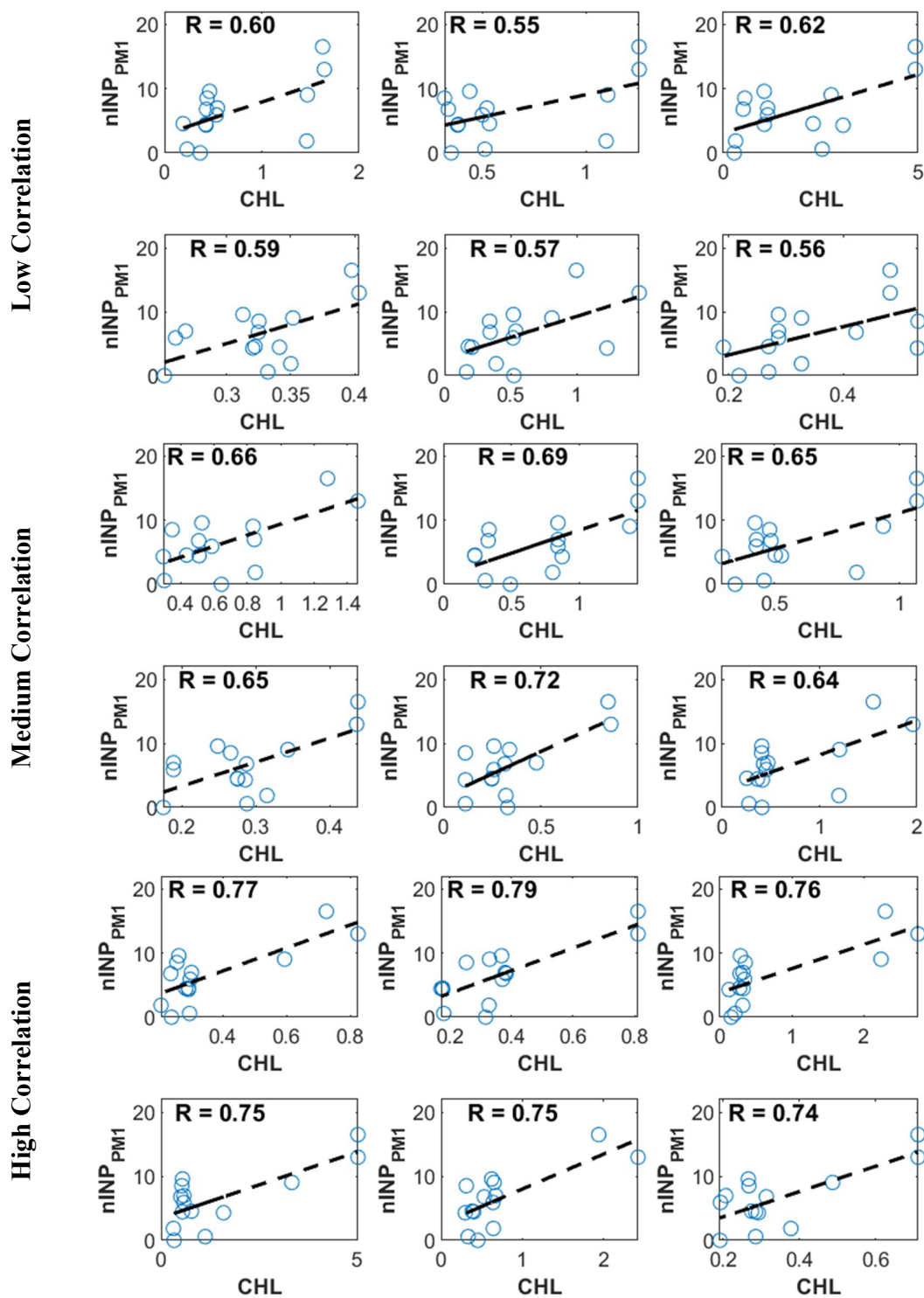


Figure S14: Scatter plots between $nINP_{PM1}$ sampled at GVB and CHL at pixels selected randomly within seawaters surrounding the Svalbard archipelago.

Category

Region 2 [73° – 78° N and 9° – 24° W]

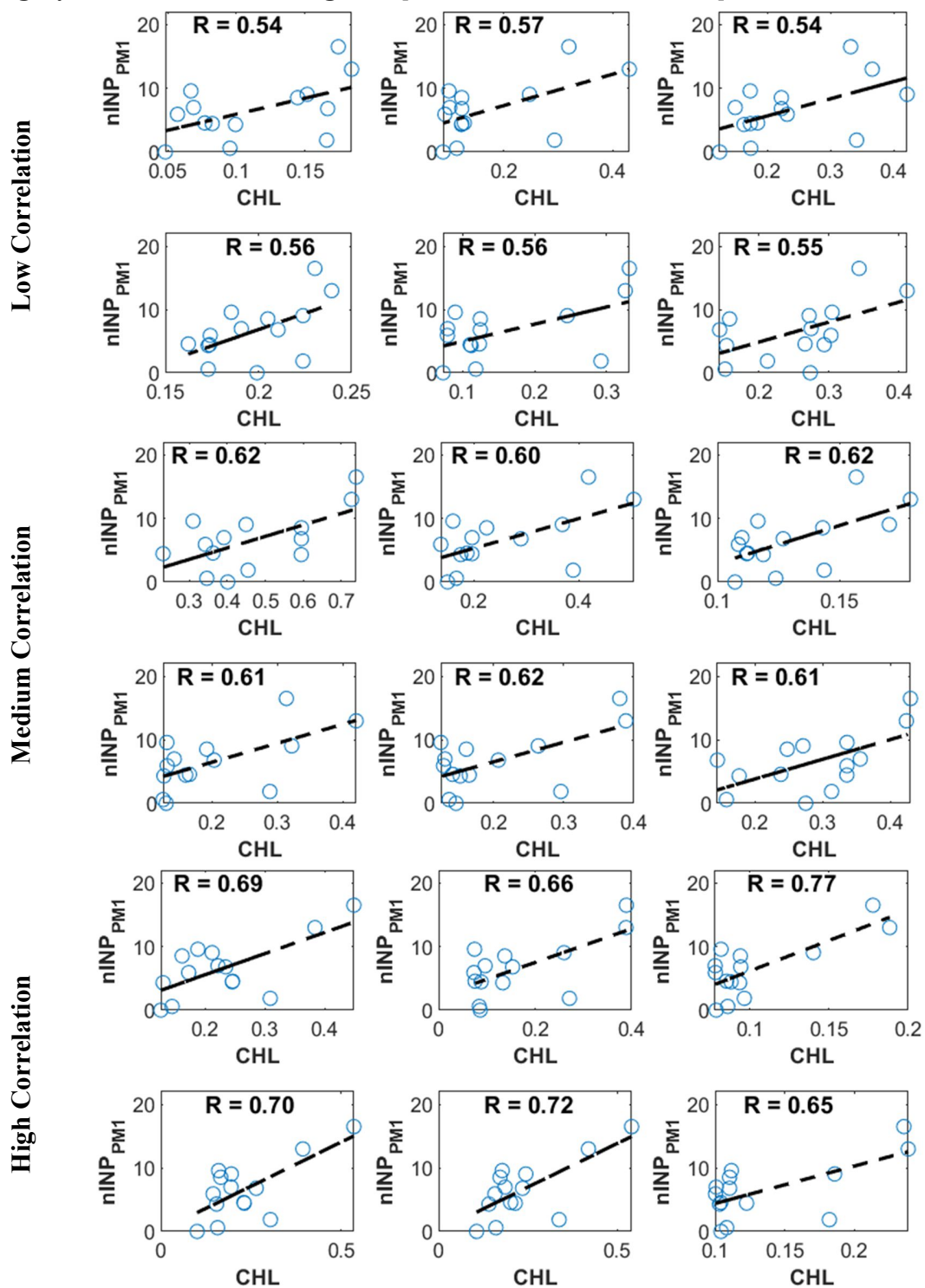


Figure S15: Same as Figure S14, but for seawaters close to the Greenland coast.

Category

Region 3 [67° – 71° N and 18° W – 0° E]

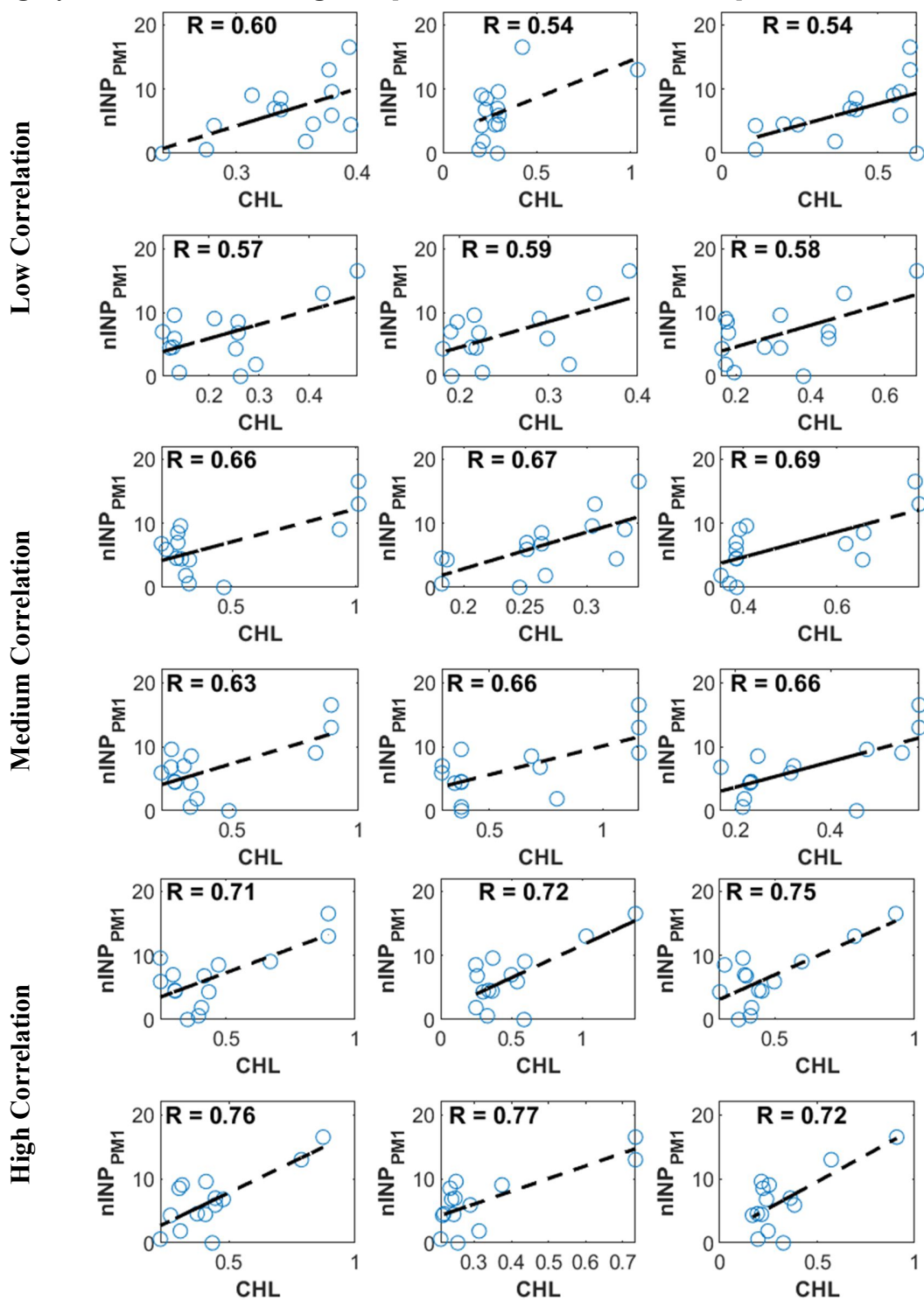


Figure S16: Same as Figure S14, but for seawaters to the northeast of Iceland.